Available online at www.sciencedirect.com
ScienceDirect
Acta Materialia 56 (2008) 4458–4469
Acta MATERIALIA
www.elsevier.com/locate/actamat

Influence of indenter angle on cracking in Si and Ge during nanoindentation

Jae-il Jang [a,*], G.M. Pharr [b,c]

[a] Division of Materials Science and Engineering, Hanyang University, Seoul 133-791, Republic of Korea
[b] Department of Materials Science and Engineering, The University of Tennessee, Knoxville, TN 37996-2200, USA
[c] Materials Science and Technology Division, Oak Ridge National Laboratory, Oak Ridge, TN 37831, USA

Received 11 January 2008; received in revised form 1 May 2008; accepted 1 May 2008
Available online 2 June 2008

Abstract

The influence of indenter angle on the nanoindentation cracking behavior of single crystal Si and Ge was systematically explored through nanoindentation experiments with a series of triangular pyramidal indenters with different centerline-to-face angles in the range 35.3–85.0°. The relationships between indentation load, crack length and indentation size and their dependence on indenter angle were carefully examined and compared with previous indentation cracking studies. The results are discussed in terms of ways to estimate fracture toughness and indentation cracking threshold loads more precisely through nanoindentation.

Keywords: Nanoindentation; Toughness; Cracking; Semiconductors

1. Introduction

Over the past three decades, indentation testing has been widely used to measure the fracture toughness of brittle materials such as glasses and ceramics. Indentation fracture toughness measurement is attractive largely because of simplicity – there is no need for complex sample preparation (e.g. machining of complex geometries and fatigue pre-cracking) that is usually required in conventional fracture toughness testing. During indentation with a sharp pyramidal indenter, the material underneath the indenter experiences highly localized stresses and strains. If a hard/brittle material is indented, these high stresses cause not only elastic–plastic deformation but also severe cracking around the indentation impression. Although indentation-induced cracking was first realized as a possible measure of fracture toughness in the late 1950s by Palmqvist [1], it was in the 1970s when the real practical importance was proposed by Lawn and colleagues [2,3] and Evans and co-workers [4,5], who worked to relate the stress intensity factor K for Vickers indentation to the observed crack dimensions. In the early 1980s, borrowing results from the expanding-cavity solution for an elastic–plastic solid, Lawn et al. [6] and then Anstis et al. [7] suggested a relation for estimating the fracture toughness (K_C) through Vickers indentation, based on the half-penny crack configuration:

$$K_C = \alpha\left(\frac{E}{H}\right)^{\frac{1}{2}}\frac{P}{c^{3/2}} \tag{1}$$

where P is the indentation load, c is the radial crack length from indentation center to crack tip, E is Young's modulus, H is the hardness, and α is a constant for a given indenter. They also suggested [6] that α is proportional to $(\cot\Psi)^{2/3}$, where Ψ is the included half-angle of the four-sided pyramidal indenter (i.e. $\Psi = 68°$). Anstis et al. [7] empirically determined the value of α as 0.016 ± 0.004 through Vickers indentation and double-cantilever beam (DCB) tests on a number of brittle materials. Although

* Corresponding author.
E-mail address: jijang@hanyang.ac.kr (J.-i. Jang).

1359-6454/$34.00 © 2008 Acta Materialia Inc. Published by Elsevier Ltd. All rights reserved.
doi:10.1016/j.actamat.2008.05.005

there have been many additional efforts to develop the method (see review articles in Refs. [8,9]) and a multitude of other formulas have been proposed that differentiate between the behavior of half-penny cracks and Palmqvist cracks [10–16], Eq. (1) remains the most popular relation for estimating toughness by Vickers indentation. Ponton and Rawlings [17,18] examined 19 different Vickers indentation toughness equations (from Eq. (1) to Tanaka's simplified equation [19]), and found that most of them have an accuracy on the order of 30%, with minor variations.

With the development of nanoindentation testing in the early 1990s [20,21], it was revealed that Eq. (1) also applies to the three-sided Berkovich indenter commonly used in nanoindentation testing, even though there is an important symmetry difference between the Vickers and Berkovich indenters (for example, see Ref. [22]). Nanoindentation also offers an advantage in that E and H in Eq. (1) can be measured directly during the test [20,23]. However, it was recognized that, at the very small loads applied in nanoindentation, a new issue arises, namely, that most brittle materials exhibit a cracking threshold below which no radial cracking occurs, i.e. nanoindentation at a load below the threshold cannot be used to estimate fracture toughness. To overcome this difficulty, Pharr and colleagues [24–25] recommended using a cube-corner indenter with a centerline-to-face angle of 35.3°, which is much sharper than the Berkovich indenter (65.3°). This recommendation was based on the fact that the sharper cube-corner indenter displaces a much larger volume of material for a given load (more than three times that of the Berkovich indenter) and thus produces higher stresses beneath the indenter [26–28]. In many studies, the cube-corner indenter has been found to be extremely effective for radial crack initiation at very small loads and is now popularly used for toughness estimation in very small volumes and thin films [29–35]. In a similar manner, three-sided pyramidal indenters with other angles have recently been employed in the cracking studies [36,37]. In general, the experimental results support Lawn et al.'s [6] suggestion that the proportionality coefficient α in Eq. (1) depends on the indenter angle. Thus, to measure indentation toughness precisely with different-angle indenters, it is very important to understand this dependency. Nevertheless, to the best of the authors' knowledge, the influence of indenter angle on cracking behavior during nanoindentation has never been systematically examined in an experimental way.

With this in mind, here the influence of the indenter angle (i.e. indenter sharpness) on indentation cracking is explored by conducting a series of nanoindentation experiments on single crystals of silicon (Si) and germanium (Ge) with a series of triangular pyramidal indenters with different centerline-to-face angles (Ψ) in the range 35.3–85.0°. The results are considered in terms of their relation to fracture toughness measurement and also to the indentation cracking threshold load, which is important in the precision micro-machining of semiconductors and other brittle materials.

2. Experimental details

Single-crystal wafers of (100) Si and (100) Ge were tested using a Nanoindenter-XP (MTS Corp., Oak Ridge, TN). Six different triangular pyramidal indenters with centerline-to-face angles Ψ (described in Fig. 1) of 35.3° (cube-corner indenter), 45.0°, 55.0°, 65.3° (Berkovich indenter), 75.0° and 85.0° were employed. The accuracy of the angle was reported by the manufacturer to be within ±0.15°. Loadcontrolled nanoindentations were performed with each indenter at various maximum loads from 1 to 100 mN and loading rates from 0.05 to 5 mN/s. For the 75.0° and 85.0° indenters, the maximum loads were increased up to 500 mN. After indentation testing, all the hardness impressions were imaged using a Leo 1525 field-emission scanning electron microscope (Carl Zeiss SMT Inc., Thornwood, NY) to measure the sizes of the contact impression and the lengths of the radial cracks emitted from their corners. It should be noted that crack-closure can occur during unloading of the indenter, and this phenomenon could affect some of the results of our analysis. We could not experimentally measure the extent of crack closure since we performed the *crack length* measurements only after unloading using magnified SEM images. That being said, however, the locations of the crack tips seemed very well defined and easy to identify in most of the micrographs.

3. Results

3.1. Indenter angle effects on load–displacement (P–h) curves

Fig. 2 shows representative examples of nanoindentation load–displacement (P–h) curves obtained at high and low peak loads (50 and 10 mN) and a constant loading/unloading rate of 0.5 mN s^{-1}. For both Si and Ge, a larger peak–load displacement and a greater proportion of irre-

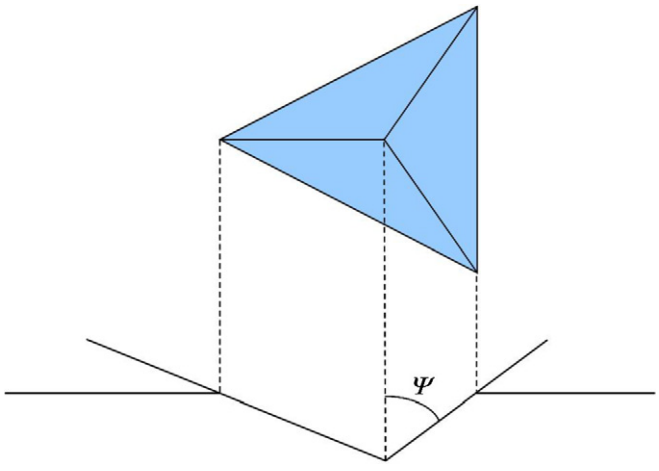

Fig. 1. Schematic illustration of the centerline-to-face angle Ψ for a three-sided pyramidal indenter.

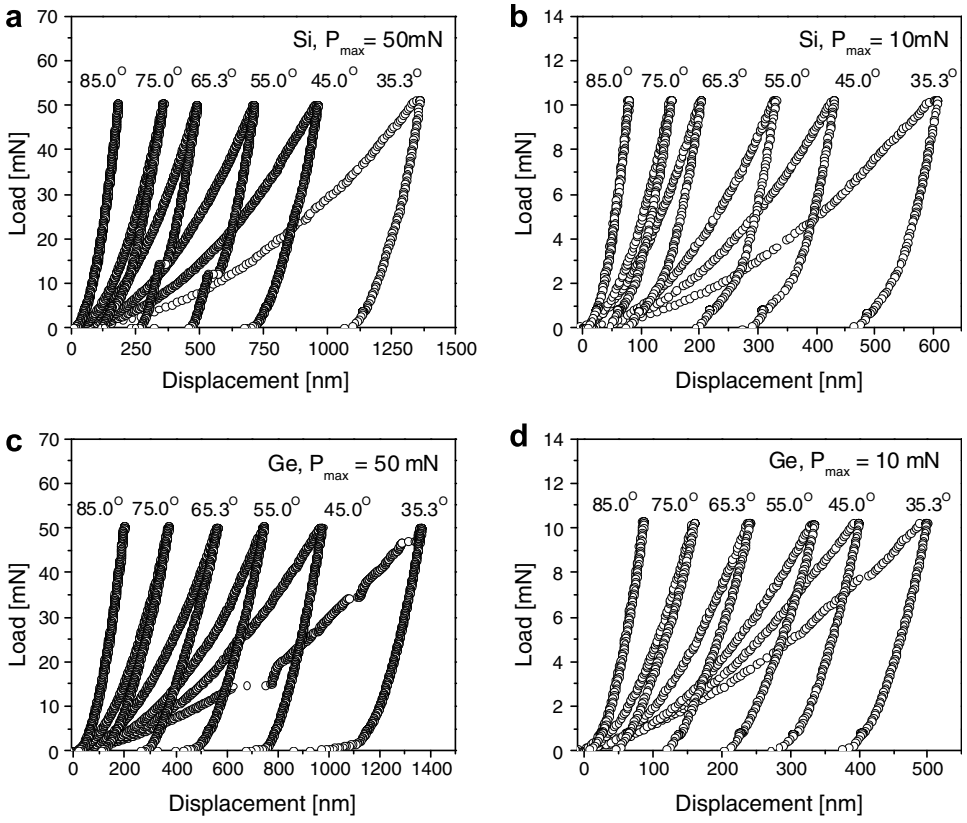

Fig. 2. Variations in load–displacement curves of Si [(a), (b)] and Ge [(c), (d)] obtained with the various indenters, and the maximum load: (a) and (c) $P_{max} = 50$ mN; (b) and (d) $P_{max} = 10$ mN. Results are from nanoindentations at a fixed loading/unloading rate 0.5 mN s^{-1}.

versible plastic deformation after unloading are observed for the sharper indenters (i.e. indenters with smaller angles). For the 85.0° indenter, contact was purely elastic, i.e. the loading and unloading curves are identical.

Since Ge has a lower fracture toughness than Si [38–43], considerable chipping and material removal was observed in the Ge tests conducted at higher loads. Thus, for very sharp cube-corner indentation ($\Psi = 35.3°$) of Ge at relatively high load (50 mN in Fig. 2), the *P–h* curve exhibits a number of excursions or "pop-in" events which correspond to chipping and material removal (to be shown later), and thus exhibits a larger peak–load displacement than that of Si. At a relatively low load (10 mN), all the *P–h* curves for Ge show a smaller peak–load displacement than for Si.

3.2. Indenter angle effects on hardness impressions and cracking behavior

Fig. 3 shows a series of scanning electron microscopy (SEM) images obtained from nanoindentations made at 50 mN with indenters with different indenter angles (Ψ) from 35.3° to 75.0°. For the 85.0° indenter, contact is purely elastic, so no remnant indentation is produced, and no image is shown. For sharper indenters, well-developed radial cracks are clearly observed, and the crack lengths gradually decrease with increasing angle. For the case of 75.0° indentation in Si, radial cracks were not detected. Note that the extruded material observed in the cube-corner indentations is due to an indentation-induced phase transformation unique to Si and Ge [26,27].

The dependences of the hardness impression size and the radial crack length on indenter angle observed in Fig. 3 are summarized in Fig. 4. In this plot, a is the size of the hardness impression measured from the indentation center to the corner and c is the crack length measured from the indentation center to the crack tip. The measurements were averaged over the three sides of the hardness impression. By the fact that the indentation size (a) is almost independent of indenter angle (Ψ), it is apparent that the indentation hardness (H) of the materials is not significantly dependent on the indenter angle. Note, however, that the hardness measured by observing the residual impression can be different from that measured by nanoindentation (theoretically equal to mean contact pressure under the maximum indentation load) due to elastic recovery during unloading [44]. For a blunter (higher angle) indenters such as the 75.0° indenter, the amount of elastic recovery is greater than for the sharper indenters.

However, the crack length (c) in Fig. 4 is strongly dependent on Ψ, showing a substantial decrease as Ψ increases. This tendency is readily explained by considering the indenter geometry. As each indenter produces almost the same projected area at a given load, the sharper indenters displace more volume and thereby produce greater local stresses to drive cracking.

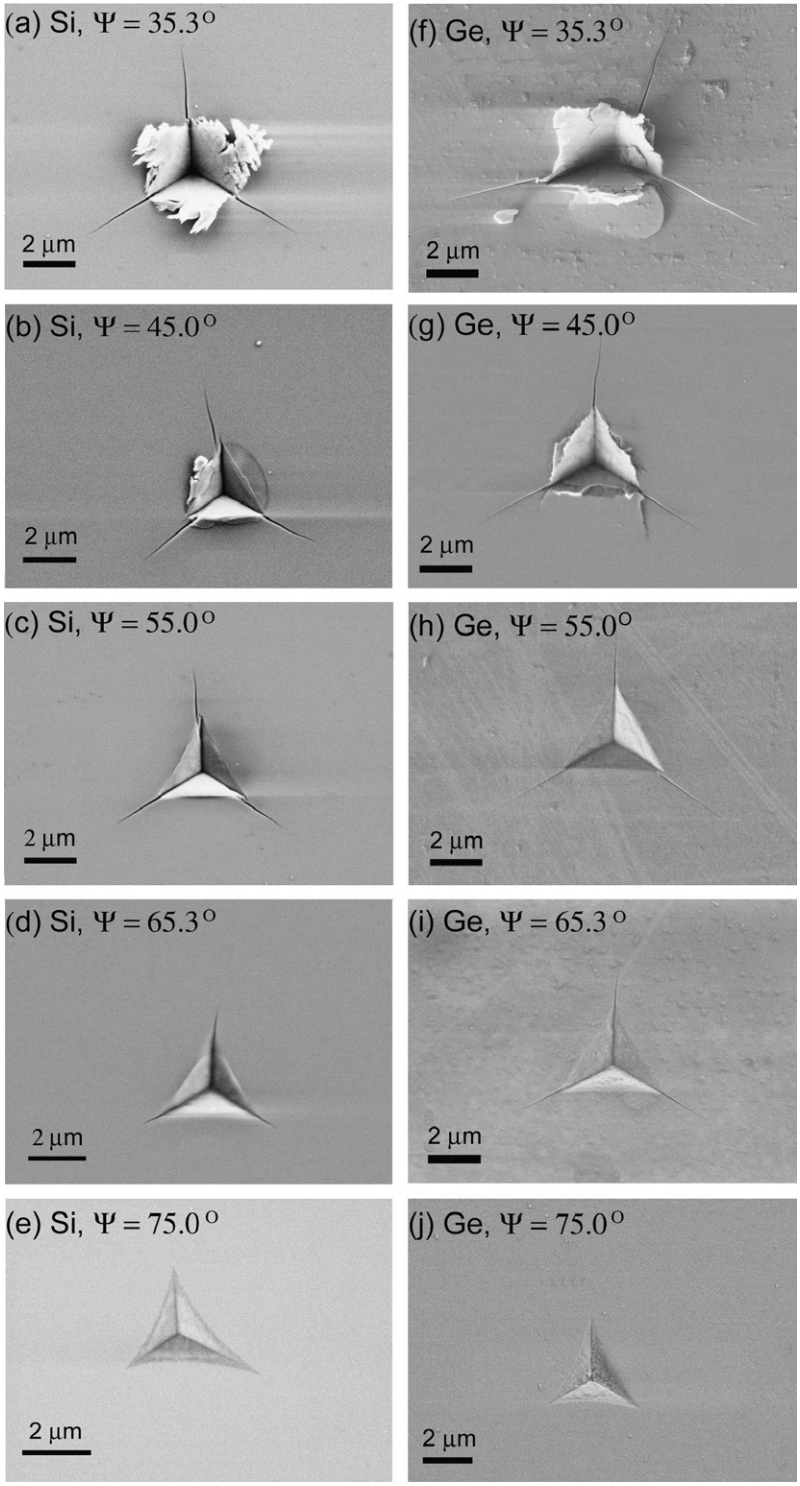

Fig. 3. SEM micrographs of nanoindentations in (a)–(e) Si and (f)–(j) Ge made with indenters of various angles at a peak load of 50 mN and loading/unloading rate 0.5 mN s^{-1}. Note that the magnification of each image is not exactly the same.

3.3. Indenter angle effects on the cracking threshold load

Similar to the crack size dependence on the indenter angle, a sharper indenter exhibits a lower cracking threshold load below which no cracking is observed. The measured threshold loads for each indenter are listed in Table 1. Fig. 5 shows SEM micrographs of the indentations made with the 75.0° indenter at a load of 500 mN. Whereas no radial cracking is seen in Si, radial cracks are clearly observed in Ge, which is more brittle than Si.

The cracking thresholds observed here are consistent with the suggestion [24,25] that a sharper indenter such

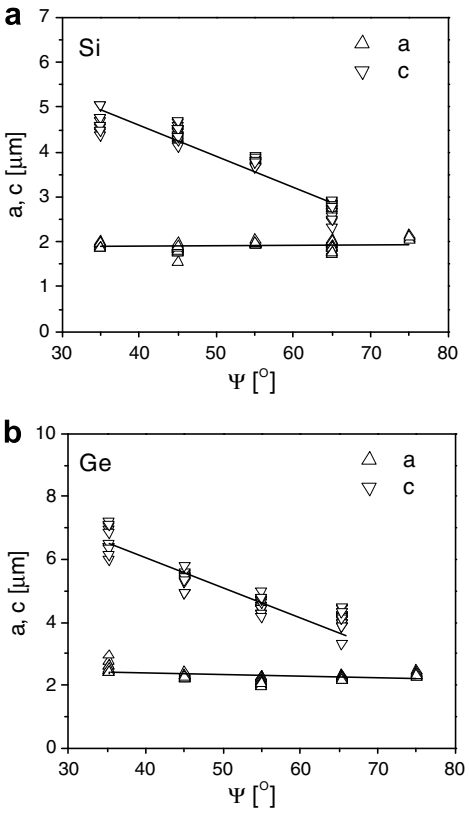

Fig. 4. Influence of indenter angle (Ψ) on the indentation size (a) and crack length (c) of nanoindentations made at a peak load of 50 mN: (a) Si and (b) Ge.

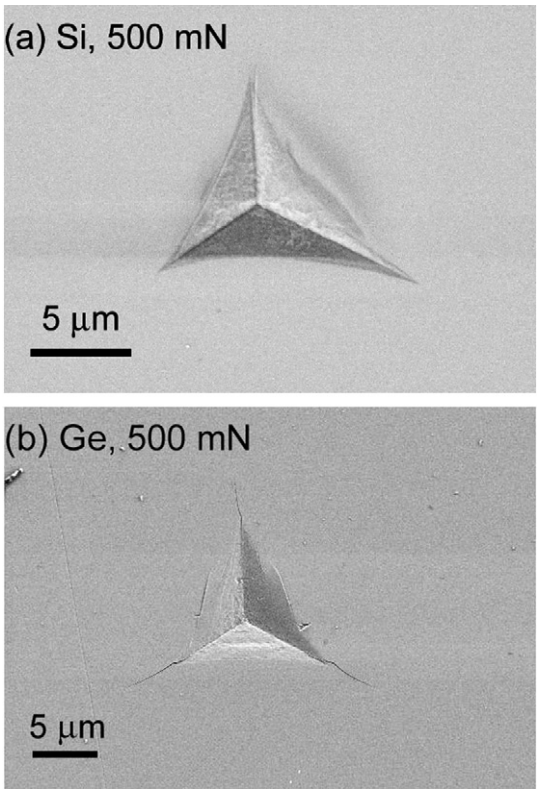

Fig. 5. SEM micrographs of nanoindentations made with the 75.0° indenter at the highest load applied in this study (500 mN): (a) Si and (b) Ge.

Table 1
Summary of threshold loads for radial cracking observed in this work

Angle (Ψ)	Radial cracking threshold load (mN)	
	Si	Ge
35.3°	<1	<1
45.0°	<1	<1
55.0°	~1	<1
65.3°	10–20	5–10
75.0°	>500	80–100
85.0°	No hardness impression	No hardness impression

as the cube-corner is useful in reducing the cracking threshold for indentation toughness measurements. Nevertheless, it is constructive to note that, at high loads, a sharper indenter frequently produces severe chipping and surface/subsurface damage, especially in very brittle materials. It is well known that the fracture toughness of Ge is not easily measured by conventional Vickers indentations because serious chipping and damage occur at a load >500 mN [42]. A similar situation was observed in the present work for nanoindentation of Ge with a Berkovich indenter at 500 mN (see Fig. 6a). This similarity between the response from the Vickers and Berkovich indenters can be expected, as the two geometries have the same area to depth ratio. When a much sharper cube-corner indenter is used, heavy chipping can occur at a load lower than the critical load for Berkovich indentation. Fig. 6b shows an SEM image of a cube-corner indentation at 100 mN (the highest load applied here for cube-corner indenter), in which the chipping and damage are clearly observed. In this study, only indentations with no or only minor chipping were taken into account for size measurement.

3.4. Peak load effects on indentation size and crack lengths

The influence of indentation load (P) on the indentation size measured from the indentation center to corner (a) and the crack length from the indentation center to crack tip (c) were systematically examined. The intrinsic indentation hardness H is simply defined as the load divided by the projected area of the indentation; thus, for a given P and a, the hardness obtained from three-sided pyramidal indentation may be expressed as

$$H = \frac{4P}{3\sqrt{3}a^2}. \tag{2}$$

Therefore, a logarithmic plot of a vs P for each indenter should yield a linear relationship with a slope of 0.5. Plots of this type are shown in Fig. 7, indicating that the linear relationship holds for all the indenters and load ranges. The correlation factors R for the linear fits are mostly >0.99. As a is independent of indenter angle in these materials (see Fig. 4), the lines in Fig. 7 overlap each other.

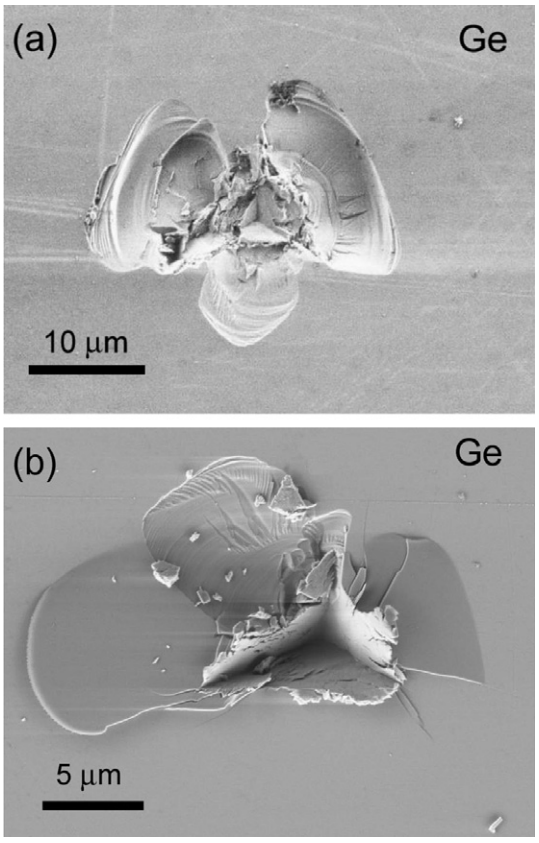

Fig. 6. Examples of chipping and surface damage for Ge observed at relatively high loads: (a) Berkovich indentation at 500 mN and (b) cube-corner indentation at 100 mN.

On the other hand, the essential features of most indentation toughness equations are based on the stress intensity factor K for a center-loaded, penny-shaped crack system (originally developed by classic fracture mechanics analysis using the stress function [45–47]):

$$K = \kappa\theta\frac{P_{\perp}}{c^{3/2}} \tag{3}$$

where $P_{\perp}$ is the indentation-induced wedging force to open the crack (proportional to indentation load P), κ is a constant approximately equal to $(2/\pi^{3/2})$, and θ is a correction factor close to 1.12 in the case of "half"-penny-shaped crack system for correcting the existence of the surface. Given that the cracks extend until the stress intensity factor is equal to the fracture toughness K_C, the indentation load should then scale as $(c^{3/2})$, i.e. $c \propto P^{2/3}$. Log–log plots of c vs P are shown in Fig. 8. The above relation is valid for all indenters that produced cracks: the slope of each plot is about 2/3 and the correlation factors R for the linear fits are mostly >0.99. In Fig. 8, the distinct difference in intercept values for each indenter implies that the indenter angle plays an important role in indentation fracture toughness measurement, as will be discussed later. Moreover, note that even for very small loads and crack lengths, the proportionality between c and $P^{2/3}$ is maintained, i.e. the system behaves as if it were penny-shaped for all loads and indenter angles.

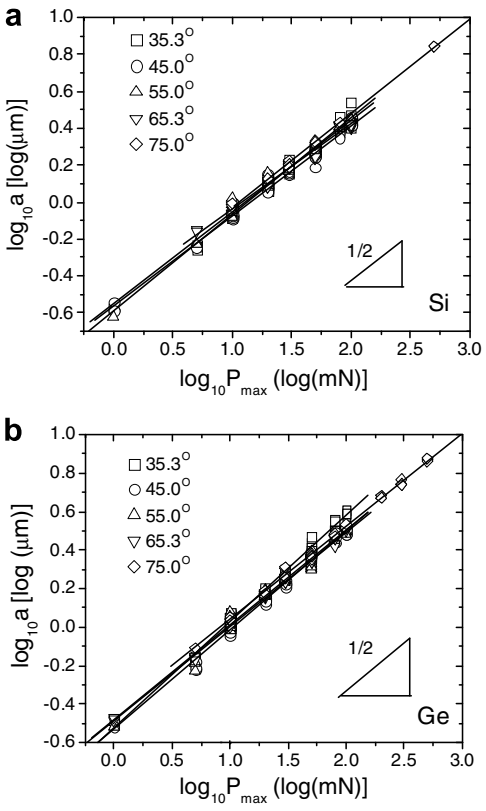

Fig. 7. Log–log plots of the indentation size (a) vs the maximum load (P_{max}): (a) Si and (b) Ge.

3.5. Rate effects on the indentation size and crack lengths

The influence of the nanoindentation loading/unloading rate on the measured crack lengths and indentation sizes were examined for all indenters, with a representative example shown in Fig. 9. No clear dependence of the sizes on the rate was observed over the range of the rates, which are typical for nanoindentation studies.

4. Indenter angle influences on toughness and cracking threshold loads

4.1. Estimation of fracture toughness

In previous sections, it was confirmed that the penny-shaped crack system can be adopted in toughness measurement within the typical nanoindentation load range, i.e. for each indenter, the $(P/c^{3/2})$ values are approximately constant (even at very small loads such as 1 and 5 mN) and almost independent of indentation load. The next and the most important step in this work is to find the dependency of α in Eq. (1) on the indenter angle. Fig. 10 shows the variation in $(P/c^{3/2})$ with the angle Ψ. The $(P/c^{3/2})$ values for both Si and Ge increase with increasing Ψ. Because the fracture toughness (K_{IC}) and Young's modulus (E) are intrinsic material properties, independent of Ψ, and the hardness (H) measured here is also independent of Ψ, α in Eq. (1) should decrease with indenter angle. Fig. 11 plots

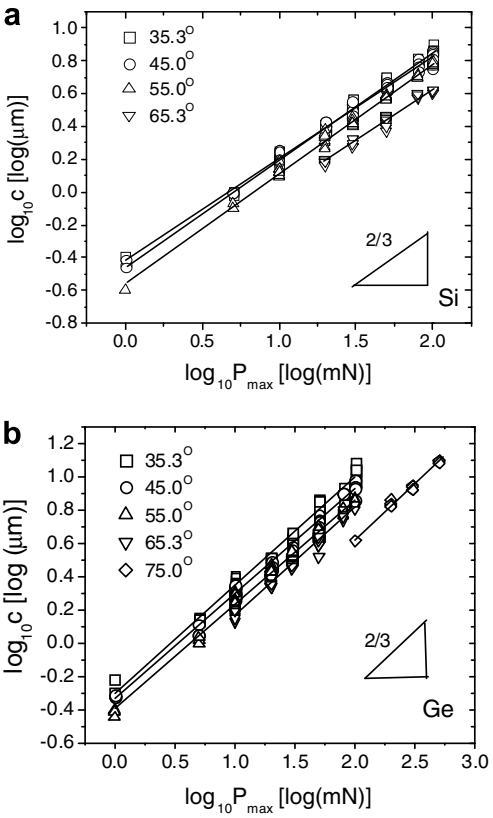

Fig. 8. Log–log plots of the crack length (c) vs the maximum load (P_{max}): (a) Si and (b) Ge.

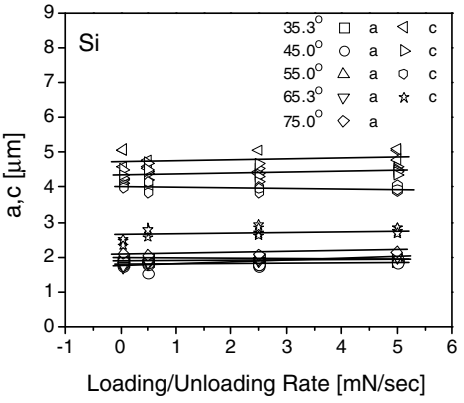

Fig. 9. An example demonstrating the dependence of the indentation size and crack length on the loading/unloading rate (nanoindentation of Si made at $P = 50$ mN). Radial cracking was not observed for the 75.0° indenter.

α vs Ψ with the fracture toughness taken as constant (i.e. $K_{IC} = 1.0$ and 0.6 MPa $m^{1/2}$ for Si and Ge, respectively [38–43]). Although α shows a wide fluctuation for a given angle, the α values obtained from Si and Ge are similar to each other and demonstrate a decreasing tendency as the angle increases, consistent with Eq. (1).

To obtain experimentally a representative value for α (for Si and Ge), the dependence of the normalized crack length $K_{IC}(H/E)^{1/2}c^{3/2}$ on the indentation peak load is plotted in Fig. 12 and summarized in Table 2 for each indenter. The relation between the normalized crack length and indentation load shows very good linearity (indicated by high values of correlation factor R) and the representative value of α (α_R) can be determined as the slope of each linear relation. The α_R for the cube-corner indenter obtained here is higher than that suggested in previous studies [24,25], probably because the values are affected by which the value of K_{IC} is assumed. If the toughness of Si is taken as 0.7 MPa $m^{1/2}$ (as in previous studies [24,25] which adapted the value from Vickers indentation studies [7,48,49]) rather than 1.0 MPa $m^{1/2}$ as used here, the α_R values would be reduced. The toughness of Si is now well accepted as 1.0 MPa $m^{1/2}$ [38–41].

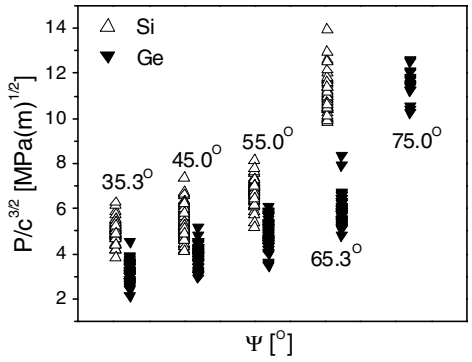

Fig. 10. Variations in $P/c^{3/2}$ value with change in the indenter angle.

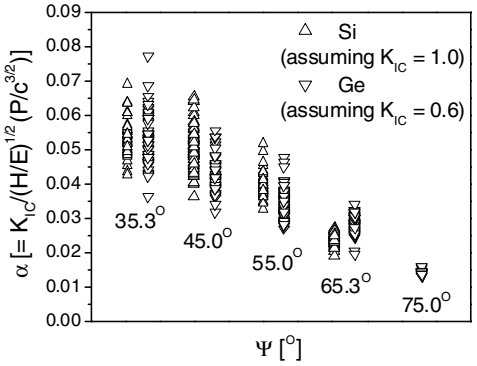

Fig. 11. Variations in stress intensity factor coefficient α with indenter angle. K_{IC} values of 1.0 and 0.6 MPa $m^{1/2}$ were used for Si and Ge, respectively.

It is instructive to compare the α_R experimentally determined for Si and Ge in this work with a theoretical value of α (α_{th}) that can be developed based on simple principles. As Eq. (1) was developed for a four-sided pyramidal Vickers indentation [6,7], here we reconsider the original analysis in Ref. [6] and modify to find an expression for α_{th} that can be applied to radial cracks produced by a three-sided pyramidal indenter. Lawn et al.'s [6] model began with the basic assumption that a small hemisphere of material is removed from an elastic half-space and plastically deformed by indentation. The irreversible strain associated with the formation of the hardness impression is accommodated by

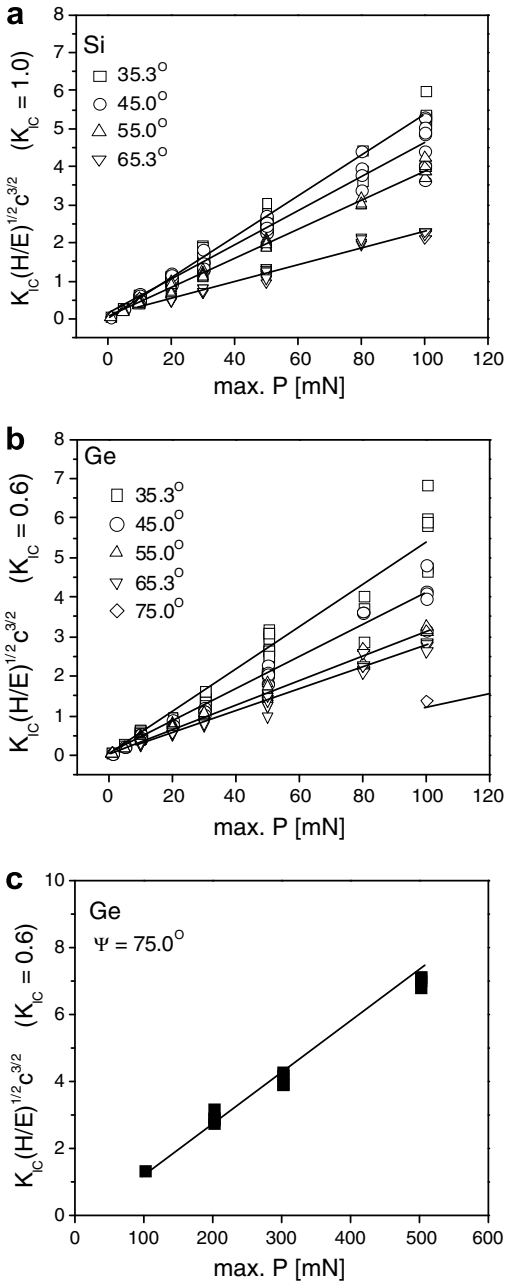

Fig. 12. Determination of representative α using the relation between the normalized crack length and the maximum load: (a) Si, (b) Ge and (c) Ge tested with the 75.0° indenter. K_{IC} values of 1.0 and 0.6 MPa $m^{1/2}$ were used for Si and Ge, respectively.

an expansion of the radius of the hemisphere so as to maintain constant volume. If δV is the volume displaced by a three-sided pyramidal indenter and V is the volume of material removed from the elastic half-space, the volumetric strain during indentation can be expressed in terms of the indenter angle Ψ as:

$$\frac{\delta V}{V} = \frac{\frac{1}{3}h\left(\frac{3\sqrt{3}}{4}a^2\right)}{\frac{1}{2}\left(\frac{4}{3}\pi b^3\right)} = \frac{3\sqrt{3}}{16\pi}\left(\frac{a}{b}\right)^3 \cot\Psi \tag{4}$$

where h is the indentation displacement into the surface, a is the indentation size measured from impression center to corner, and b is the radius of the plastic zone which is assumed hemispherical. The hemisphere is then elastically compressed back to its original radius by hydrostatic compression. The pressure required to do this is

$$p_b = B\frac{\delta V}{V} = \frac{\sqrt{3}E}{16\pi(1-2\nu)}\left(\frac{a}{b}\right)^3 \cot\Psi \tag{5}$$

where B and ν are the bulk modulus and Poisson's ratio, respectively. The compressed hemisphere is then reinserted into the cavity and allowed to expand. By analogy to Eshelby's spherical inclusion problem [50], the pressure on the relaxed hemisphere will reduce to a fraction of p_b. The remaining pressure p_r results from the constraint by the surrounding matrix. From Eshelby [50], the reduction in pressure on the relaxed hemisphere is expressed as

$$p_r = p_b\frac{2(1-2\nu)}{3(1-\nu)} = \frac{\sqrt{3}E}{24\pi(1-\nu)}\left(\frac{a}{b}\right)^3 \cot\Psi. \tag{6}$$

Consequently, the constraint on the relaxed hemisphere gives rise to residual stresses that drive crack extension. The magnitude of the crack wedging force F_r is obtained by integrating the horizontal stress components over the cross-section of the hemisphere containing the crack plane:

$$F_r = p_r\left(\frac{\pi}{2}b^2\right) = \frac{\sqrt{3}E}{48(1-\nu)}\left(\frac{a^3}{b}\right)\cot\Psi. \tag{7a}$$

From Eq. (2), Eq. (7a) can be rewritten as

$$F_r = \frac{P}{36(1-\nu)}\left(\frac{E}{H}\right)\left(\frac{a}{b}\right)\cot\Psi. \tag{7b}$$

Using the stress intensity factor for the center-loaded half-penny-crack system (described in Eq. (3)) and assuming F_r in Eq. (7b) is equal to $P_\perp$ in Eq. (3), the stress intensity factor resulting from the residual wedging force can be written as

$$K \approx \frac{1.12}{18\pi^{3/2}(1-\nu)}\left(\frac{E}{H}\right)\left(\frac{a}{b}\right)\cot\Psi\frac{P}{c^{3/2}}. \tag{8}$$

Table 2
Summary of α values determined experimentally (α_R) and analytically (α_{th})

Angle (Ψ)	α_R (from $K_{IC}(H/E)^{1/2}c^{3/2} = \alpha_R P_{max}$)				α_{th} (for Si and Ge)
	For Si	R value	For Ge	R value	
35.3°	~0.0533	0.99249	~0.0537	0.97525	~0.0569
45.0°	~0.0475	0.98034	~0.0415	0.98642	~0.0452
55.0°	~0.0390	0.99689	~0.0317	0.99169	~0.0357
65.3°	~0.0237	0.98286	~0.0279	0.99145	~0.0269
75.0°	No crack	No crack	~0.0147	0.99187	~0.0188

Hill's expanding cavity solution [51] can be used to provide a description of H/E as a function of b/r, where r is the cavity radius. A power-law fitting of the relationship between H/E vs b/r for various ceramics and glasses [52] in combination with $v = 0.25$ gives [6,53]:

$$\frac{b}{r} \approx 0.675\left(\frac{E}{H}\right)^{\frac{1}{2}}. \tag{9}$$

If the volume of the three-sided pyramidal indentation is allowed to equal the volume of the cavity ($=2\pi r^3/3$), one obtains

$$r = a\left(\frac{3\sqrt{3}\cot\Psi}{16\pi}\right)^{\frac{1}{3}}. \tag{10}$$

By combining Eq. (9) and Eq. (10),

$$\frac{a}{b} \approx 1.48\left(\frac{16\pi}{3\sqrt{3}}\right)^{\frac{1}{3}}\left(\frac{H}{E}\right)^{\frac{1}{2}}(\cot\Psi)^{-\frac{1}{3}}. \tag{11}$$

If Eq. (11) is used for a/b in Eq. (8), the stress intensity factor becomes:

$$K \approx \frac{0.0352}{(1-v)}(\cot\Psi)^{\frac{2}{3}}\left(\frac{E}{H}\right)^{\frac{1}{2}}\frac{P}{c^{3/2}} \tag{12}$$

and comparison to Eq. (1) yields:

$$\alpha_{th} = \frac{0.0352}{(1-v)}(\cot\Psi)^{\frac{2}{3}}. \tag{13}$$

Eq. (13) indicates that α is theoretically dependent not only on indenter angle Ψ, but also on material parameters such as Poisson's ratio v which were not contained in Lawn et al.'s original analysis. When Poisson's ratio is taken as 0.22 for both Si and Ge, the calculated values of α_{th} for all the indenters are listed in Table 2. It is found that α_{th} is in a good agreement with empirically obtained α_R, at least for Si and Ge. This suggests that Eq. (12) may be useful in estimating fracture toughness by nanoindentation with various indenter angles. To explore this possibility, the K_C values estimated from Eq. (12) are plotted as a function of Ψ in Fig. 13. The material parameters used in the evaluation were $E = 165$ GPa, $H = 12.5$ GPa for Si, $E = 140$ GPa, $H = 10.5$ GPa for Ge (all of which were obtained from nanoindentation by the Oliver–Pharr method [20,23]), and $v = 0.22$ for both materials. Except for the case of $\Psi = 75.0°$ in Ge, the estimated values of fracture toughness match well with the values obtained in conventional fracture-toughness testing, which generally lie in the range ~0.9–1.25 MPa $m^{1/2}$ for Si [38–41] and 0.6 MPa $m^{1/2}$ for Ge [42,43]. Thus, Eq. (12) appears to be reasonably applicable to toughness estimation, at least for Si and Ge and for the most of the indenters used in this work.

Although why Eq. (12) does not work well for the 75.0° indenter is not yet fully understood, it may be at least partially explained by the elasticity-dominated nature of indentation with such a high-angle indenter. As shown in Figs. 2, 3 and 5, for high-angle indenters, the plastic portion in P–h curve is very small, and elastic sink-in behavior is observed at the residual indentation edge. As Eq. (12) is based on Hill's expanding-cavity solution [51], it may not be appropriate when elastic behavior is so dominant. Also, according to Eq. (11), the indentation size a is approximately equal to the plastic zone radius b when $\Psi = 65.3°$, and much larger than b when $\Psi = 75.0°$. Hence, the assumption of a hemispherical plastic zone under the contact and thus the dependence of K on $(\cot\Psi)^{2/3}$ may no longer be maintained when $\Psi = 75.0°$. In addition, plasticity may also play an important role in the way it influences and promotes the nucleation and initial formation of the cracks.

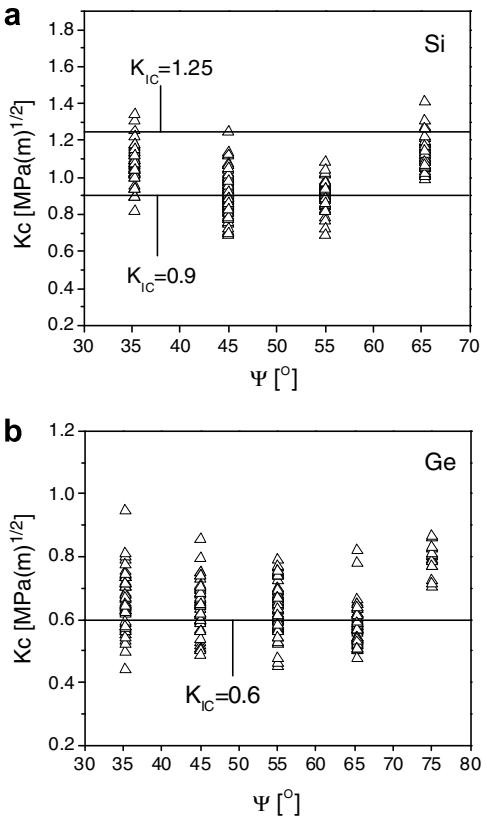

Fig. 13. Fracture toughness of: (a) Si and (b) Ge, estimated by Eq. (12) for each indenter.

We also wish to note that it is well-documented that the indentation of Si and Ge, it is associated wit a volume-reducing phase transformation [26,27]which could play a role in the determining the stresses that drive indentation cracking. However, based on the observations here, we have not found any evidence that the phase transformation plays a significant role, possibly because only a small fraction of the volume can be accommodated by it, especially for the sharper indenters.

4.2. Prediction of cracking threshold loads

Attention now turns to the cracking threshold phenomenon. Lawn and Marshall [54] discussed the importance of the hardness-to-toughness ratio H/K in predicting how

deformation and fracture compete with each other during indentation. Attention here will also be paid to the competition of deformation and fracture and thus to the ratio c/a where c and a are representative measures for K and H, respectively.

Before starting the analysis, an important issue regarding the c/a ratio must be considered; specifically, whether K ceases to be proportional to $(P/c^{3/2})$ if the c/a ratio is <2.5 [10–16]. For example, Niihara et al. [10] proposed that when c/a is <2.5, P ceases to be proportional to $c^{3/2}$ for Vickers indentation of brittle materials, and thus that Eq. (1) cannot be used for toughness measurement. With this in mind, the change in c/a as a function of indentation load was investigated, with the results shown in Fig. 14. Somewhat surprisingly, in most cases of relatively low load indentations (<50 mN) with the 35.3–65.3° indenters and even in the case of high loads indentations with the 75.0° indenter, the c/a value is <2.5, while the $(P/c^{3/2})$ values are almost independent of the load (see Fig. 8). Thus, the proportionality between P and $c^{3/2}$, i.e. Eq. (1), is maintained even for the small c/a values observed here, making it possible to estimate the fracture toughness and cracking threshold behavior by very low load nanoindentation beyond the limitation of conventional indentation toughness measurement in which radial cracks are required to be "well-developed" ($c/a \geqslant 2.5$).

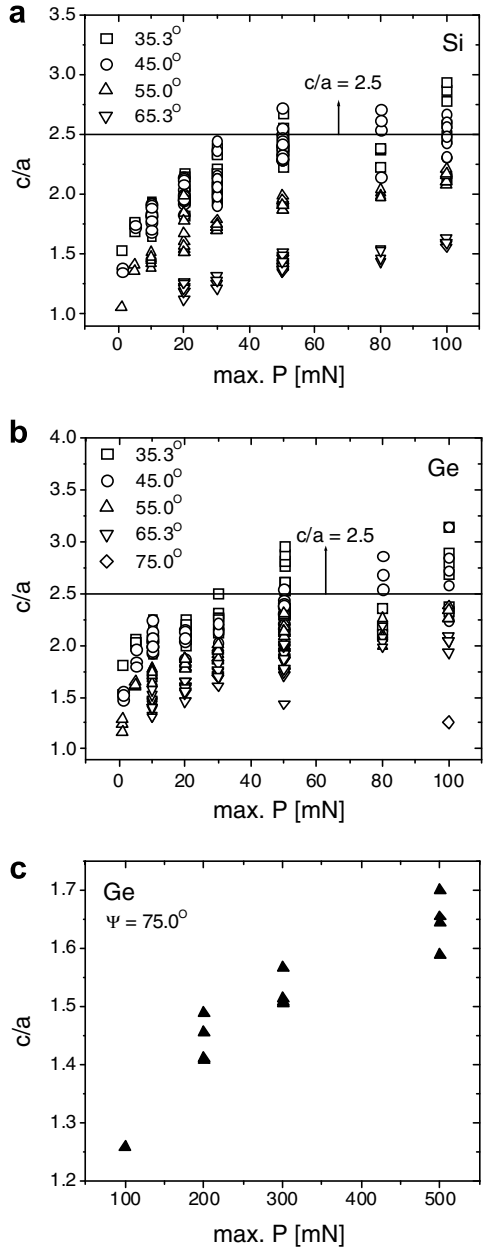

Fig. 14. Variation of the crack-length-to-indent-size ratio (c/a) with the maximum load: (a) Si, (b) Ge and (c) Ge tested with the 75.0° indenter.

As Eq. (1) appears to work even in the case where c/a is <2.5, a simple and practical way to predict the cracking threshold load can be developed as follows. By reformulating Eqs. (1) and (2), the expression for the relationship between (c/a) and the indentation load P may be written as

$$\frac{c}{a} = mP^{\frac{1}{6}} \tag{14}$$

where

$$m = \left(\frac{3\sqrt{3}}{4}\right)^{\frac{1}{2}} \alpha^{\frac{2}{3}} \left(\frac{E}{H}\right)^{\frac{1}{3}} H^{\frac{1}{2}} \left(\frac{1}{K_C}\right)^{\frac{2}{3}}. \tag{15}$$

Note that the value m is constant for a given indenter angle and material. According to Eq. (15), if α is really dependent on $(\cot\Psi)^{2/3}$, the value m should depend on $(\cot\Psi)^{4/9}$.

Based on Eq. (14), a simple and practically useful way to predict the cracking threshold load is suggested. If c/a values can be experimentally measured at loads higher than the cracking threshold load, the m value in Eq. (14) can be determined by power-law fitting c/a vs P. Then, one can estimate the cracking threshold load by extrapolating the power-law relation to $c/a = 1$. For example, an analysis for 55.0° indentation of Si is provided in Fig. 15. The c/a values vs load P were fit to Eq. (14) over whole load range, and a cracking threshold load of approximately 1 mN resulted by extrapolating the power-law curve to $c/a = 1$ (see Fig. 15a). The high-resolution SEM image (×140,000) of an indentation at 1 mN (Fig. 15b) shows the initiation of a small radial crack (with a length of about 10 nm) at an impression corner. The cracking threshold loads of Si (and Ge) predicted by this method using data obtained in the load range from 50 to 100 mN are 0.289 (and 0.226) mN, 0.326 (and 0.267) mN, 1.054 (and 0.597) mN, 6.310 (and 1.286) mN for $\Psi = 35.3°$, 45°, 55° and 65.3°. These predicted values agree reasonably well with the experimental values (listed in Table 1).

On the other hand, if the cracking threshold load is known for a certain indenter angle, there is a simple way to predict the threshold loads for other indenter angles. As elaborated above, the radial cracking threshold load P_C is roughly estimated by assuming that $P = P_C$ when $c/a = 1$. By reformulating Eqs. (1) and (2), the expression for P_C can be written as

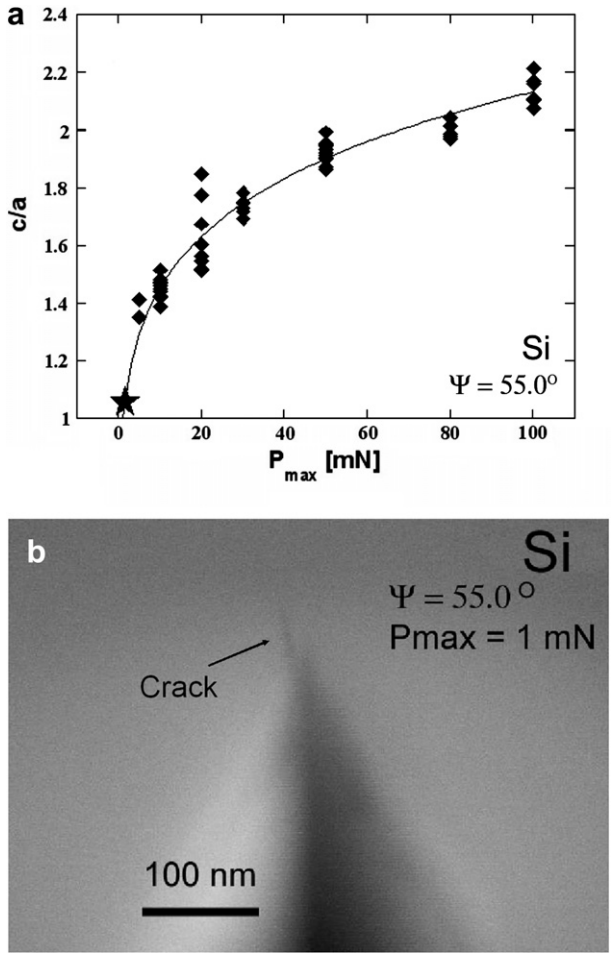

Fig. 15. An example (for $\Psi = 55.0°$) showing how the cracking threshold can be estimated by Eq. (14): (a) polynomial fitting of c/a against the maximum load; (b) high-resolution SEM micrograph (×140,000) of the nanoindentation made with the 55.0° indenter at $P = 1$ mN.

$$P_C = \left(\frac{4}{3\sqrt{3}}\right)^3 \left(\frac{1}{\alpha}\right)^4 \left(\frac{H}{E}\right)^2 \left(\frac{K_C}{H}\right)^3 K_C. \tag{16}$$

Because H, E and K_C are independent of indenter angle (for Si and Ge), and α is a function of $(\cot \Psi)^{2/3}$, P_C should be proportional to $(\tan \Psi)^{8/3}$. So, if P_{C1} is known for one indenter angle Ψ_1, P_{C2} for another indenter angle Ψ_2 can be predicted as

$$P_{C2} = P_{C1} \left(\frac{\tan \Psi_2}{\tan \Psi_1}\right)^{\frac{8}{3}}. \tag{17}$$

According to Eq. (17), the cracking threshold loads for Berkovich indentation will be approximately 20, 8, and 3 times greater than those for 35.3°, 45.0° and 55.0° indentations, respectively. The experimental values in Table 1 support this.

5. Conclusions

The influences of indenter angle on the nanoindentation cracking behavior of single crystal (100) Si and (100) Ge were systematically investigated by nanoindentation experiments with a series of triangular pyramidal indenters with different centerline-to-face angles varying from 35.3° to 85.0°. For each of the indenters, $(P/c^{3/2})$ values were essentially constant, even at very low loads and thus at very small crack-length-to-indent-size ratios c/a. In addition, the crack length decreased with increasing indenter angle, while the indent size and hardness was independent of angle. Based on these observations, new ways to estimate the fracture toughness and the cracking threshold loads are suggested.

It is hoped that these results and observations will be valuable for developing more precise ways to estimate fracture toughness by nanoindentation. Nevertheless, some important questions remain, such as: how can a half-penny-shaped crack system be operative for three-sided pyramidal indentation, despite the difference in symmetry? Is there a more precise expression for the stress intensity factor for three-sided pyramidal indentation? Most importantly, many more materials (especially materials showing work-hardening behavior and thus a hardness dependency on the angle) must be tested to evaluate critically the applicability of the methods.

Acknowledgements

This research was sponsored by National Science Foundation under Grant No. DMR-0203552 and by Korean Government, MOEHRD under the Korea Research Foundation Grant (No. KRF-2006-331-D00273).

References

[1] Palmqvist S. Jernkontorets Ann 1957;141(5):300.
[2] Lawn BR, Swain MV. J Mater Sci 1975;10:113.
[3] Lawn BR, Fuller ER. J Mater Sci 1975;10:2016.
[4] Evans AG, Wilshaw TR. Acta Metall 1976;24:939.
[5] Evans AG, Charles EA. J Am Ceram Soc 1976;59:371.
[6] Lawn BR, Evans AG, Marshall DB. J Am Ceram Soc 1980;63:574.
[7] Anstis GR, Chantikul P, Lawn BR, Marshall DB. J Am Ceram Soc 1981;64:533.
[8] Cook RF, Pharr GM. J Am Ceram Soc 1990;73:787.
[9] Sakai M, Bradt RC. Int Mater Rev 1993;38:53.
[10] Niihara K, Morena R, Hasselman DPH. J Mater Sci Lett 1982;1:13.
[11] Lankford J. J Mater Sci Lett 1982;1:493.
[12] Niihara K. J Mater Sci Lett 1983;2:221.
[13] Laugier MT. J Am Ceram Soc 1985;68:C51.
[14] Shetty DK, Wright IG. J Mater Sci Lett 1986;5:365.
[15] Laugier MT. J Mater Sci Lett 1987;6:897.
[16] Li Z, Ghosh A, Kobayashi AS, Bradt RC. J Am Ceram Soc 1989;72:904.
[17] Ponton CB, Rawlings RD. Mater Sci Technol 1989;5:865.
[18] Ponton CB, Rawlings RD. Mater Sci Technol 1989;5:961.
[19] Tanaka K. J Mater Sci 1987;22:1501.
[20] Oliver WC, Pharr GM. J Mater Res 1992;7:1564.
[21] Pharr GM, Oliver WC. MRS Bull 1992;17:28.
[22] Dukino RD, Swain MV. J Am Ceram Soc 1982;75:3299.
[23] Oliver WC, Pharr GM. J Mater Res 2004;19:3.
[24] Pharr GM. Mater Sci Eng A 1998;253:151.
[25] Harding DS, Oliver WC, Pharr GM. Mater Res Soc Symp Proc 1995;356:663.

[26] Jang JI, Lance MJ, Wen S, Tsui TY, Pharr GM. Acta Mater 2005;53:1759.
[27] Jang JI, Lance MJ, Wen S, Pharr GM. Appl Phys Lett 2005;86:131907.
[28] Jang JI, Yoo BG, Kim JY. Appl Phys Lett 2007;90:211906.
[29] Scharf TW, Deng H, Barnard JA. J Vac Sci Technol A 1997;15:963.
[30] Volinsky AA, Vella JB, Gerbeich WW. Thin Solid Films 2003;429:201.
[31] Morris DJ, Cook RF. Mater Res Soc Symp Proc 2003;766. E.9.3.
[32] Kese K, Rowcliffe DJ. J Am Ceram Soc 2003;86:811.
[33] Cook RF, Morris DJ, Thurn J. Mater Res Soc Symp Proc 2004;795. U.4.1.
[34] Morris DJ, Cook RF. J Am Ceram Soc 2004;87:1494.
[35] Scholz T, Schneider GA, Muñoz-Saldaña J, Swain MV. Appl Phys Lett 2004;84:3055.
[36] Field JS, Swain MV, Dukino RD. J Mater Res 2003;18:1412.
[37] Morris DJ, Myers SB, Cook RF. J Mater Res 2004;19:165.
[38] Chen CP, Leipold MH. Am Ceram Soc Bull 1980;59:469.
[39] Tsai YL, Mecholsky Jr JJ. J Mater Res 1991;6:1248.
[40] Fitzgerald AM, Daukardt RH, Kenny TW. Sensor Actuat A 2000;83:194.
[41] Ballarini R, Mullen RL, Yin Y, Kahn H, Stemmer S, Heuer AH. J Mater Res 1997;12:915.
[42] Lemaitre P. J Mater Sci Lett 1988;7:895.
[43] Jaccodine RJ. J Electrochem Soc 1963;110:524.
[44] Cheng YT, Li Z. J Mater Res 2000;15:2830.
[45] Lawn BR. Fracture of brittle solids. 2nd ed. Cambridge, UK: Cambridge University Press; 1993. p. 35.
[46] Sneddon IN. Proc Roy Soc London Ser A 1946;187:229.
[47] Paris PC, Sih GC. ASTM STP 1965;381:30.
[48] Lawn BR, Hockey BJ, Wiederhorn SM. J Mater Sci 1980;15:1207.
[49] Lawn BR, Marshall DB, Chantikul P. J Mater Sci 1981;16:1769.
[50] Eshelby JD. Pro Roy Soc A 1957;241:376.
[51] Hill R. The mathematical theory of plasticity. Oxford, UK: Oxford University Press; 1950 [chapter V].
[52] Chiang SS, Marshall DB, Evans AG. J Appl Phys 1982;53:298.
[53] Harding DS. PhD thesis. Rice University; 1995. p. 28.
[54] Lawn BR, Marshall DB. J Am Ceram Soc 1979;62:347.